

## Framework and Numerical Algorithm for a Phase Field Fracture Model

S. Karthik<sup>1,\*</sup>, A. Nasedkina<sup>2</sup>, A. Nasedkin<sup>2</sup> and A. Rajagopal<sup>1</sup>

<sup>1</sup>*Department of Civil Engineering, Indian Institute of Technology  
Hyderabad, India.*

<sup>2</sup>*Department of Mathematical Modeling, Southern Federal University,  
Rostov-On-Don, Russia.*

*Received 28 September 2021; Accepted (in revised version) 27 July 2022.*

---

**Abstract.** A phase field fracture model for quasi-brittle material in 2D is implemented in Abaqus software. The phase field damage variables 0 and 1 define undamaged and damaged regions of the material and simplify crack surface tracking. On the other hand, one has to use a fine spatial discretization for the smooth distribution of the phase field variable regularized by a small length scale parameter, which makes the method computationally expensive. At the fully damaged regions both the stiffness and stress reach zero. The displacements and damage are determined by a staggered approach, and a few standard benchmark fracture problems are used to demonstrate the work of the phase field fracture model under consideration.

**AMS subject classifications:** 65M10, 78A48

**Key words:** Phase field method, fracture, sharp crack, staggered approach and nonlinear finite element method.

---

### 1. Introduction

Fracture in engineering materials and structures is one of the most common modes of failure, and it is essential to check for a possible fracture and to prevent the progress of cracks in the material while designing a structure. Therefore, it is important to understand the failure behavior of various materials. Since experimental tests can be expensive and sometimes impossible to do, numerical models have gained a lot of interest in recent years. To predict the fracture failure, various numerical methods and approaches have been developed. Griffith [12] proposed a theory of brittle fracture, where the crack propagation is determined based on the energy requirements to create new crack surfaces. Nevertheless, this theory cannot predict the crack nucleation and other phenomena such as crack kinking and branching.

---

\*Corresponding author. *Email address:* karth7@gmail.com (S. Karthik)

Numerical fracture models can be considered in continuous and discontinuous settings by using the tools and methods of continuum damage mechanics, linear elastic fracture mechanics [12], and cohesive zone models [10]. Such approaches require additional criteria for crack initiation and propagation [6] and for crack branching [7]. Recent developments are focused on non classical theories, making use of length scale parameters to regularize solutions. They have built-in criteria to predict the onset of crack and produce mesh independent results for crack propagation. Hence, there is an increased interest and popularity for approaches such as the phase field models [9, 16] and peridynamic models [13]. The phase field models are based on the energy minimization principle and can automatically predict the crack initiation, growth and coalescence. Such models can also show the branching and merging of different cracks without using any additional criteria. The 2D model considered in this paper can be easily extended to three-dimensional ones since numerical implementation is straightforward in any dimension. Along with these advantages, the method has a few drawbacks. In particular, it requires a fine mesh to accurately solve the gradient terms present in the model, so that the computational cost is high. Besides, in the case of dynamic loading, the problem of the crack tip leads to inaccurate prediction of the crack velocity.

The first phase field model for modeling fracture – the isotropic second-order phase field fracture model – has been developed by Francfort and Marigo [11] by considering the regularized approximation given by Bourdin *et al.* [9]. Amor *et al.* extended it an anisotropic model, where the elastic energy was split into volumetric and deviatoric parts in order to prevent compressive loading cracks. A higher order phase field model proposed by Borden *et al.* [8], improved the computational cost of numerical methods. Karthik *et al.* [14] compared the phase field and gradient enhanced damage models. Kasirajan *et al.* [15] applied a  $C^1$ -continuous natural neighbor Galerkin method to the phase field models and showed its advantages over the standard finite element method. An extension to solve the dynamic loading in brittle materials using a hybrid phase field method [1] was studied by Raghu *et al.* [17]. We also note an exhaustive literature on finite element methods used in material phase field models given in [18].

Although the phase field method has been used by several authors for predicting crack propagation, few of the standard functions are improvised to match the actual behaviour. The degradation function for the strain energy  $g(\phi)$  was taken as a linear  $(1 - \phi)$  or quadratic function  $(1 - \phi)^2$ . But, in order to correct the energy degradation in actual computations, we have considered a higher order polynomial — viz.  $(1 - 10\phi^3 + 15\phi^4 - 6\phi^5)$ . The use of this polynomial can be better explained by Fig. 1. It is known that for lower damage values located in the interval  $[0, 0.3]$ , the degradation functions used in literature show up to 50% in the energy reduction. It is not possible in actual scenario since only 10% of energy can be reduced up to this point. However, such dynamics is correctly represented by the degradation function chosen in this paper. A hybrid formulation is employed where the computational time is reduced by considering the history parameter  $H$  in the phase field evolution equation and the linear balance of momentum equation is retained for solution of displacements. This also leads to the effective use of staggered algorithm for solving the phase field method.

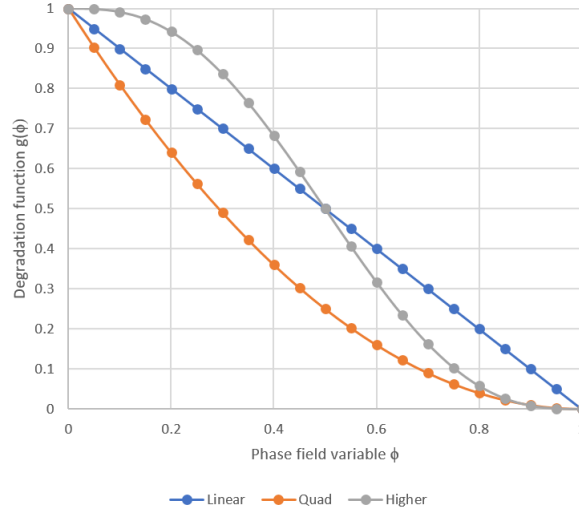


Figure 1: Energy degradation functions.

Thus unlike linear and quadratic functions, the degradation function considered in this paper, reduces the elastic energy only after a certain crack phase field value is reached. The phase field models are based on the minimization of the free energy functional with respect to displacement vectors  $\mathbf{u}$  and the crack phase field  $\phi$  to obtain partial differential evolution equations. These governing equations are solved by finite element approximations in the weak form to obtain residual vectors. The linearization of the residual vectors produces a stiffness matrix. They are solved by the Newton-Raphson method.

The structure of the paper is as follows. Section 2 contains the phase field model proposed. Section 3 is devoted to the numerical implementation and describe an algorithm for solving phase field models. A few standard examples in Section 4 demonstrate the works of the phase field model under consideration.

## 2. A Phase Field Model

Fig. 2 shows a body  $\mathcal{B}$  with a sharp crack  $\Gamma$  and diffused crack  $\Gamma_l$ . The external volume boundary is denoted by  $\partial \mathcal{B}$ . The crack propagation in the body is governed by the minimization of the total energy functional

$$E(\mathbf{u}, \Gamma) = \psi_s + \psi_f - P, \quad (2.1)$$

where  $\psi_s$ ,  $\psi_f$  and  $P$  respectively denote the strain energy, fracture energy, and the energy of external forces defined by

$$\psi_s = \int_{\mathcal{B}} \psi_0(\boldsymbol{\varepsilon}) dV, \quad \psi_f = \int_{\Gamma} G_c dA, \quad P = \int_{\mathcal{B}} \mathbf{b} \cdot \mathbf{u} dV + \int_{\partial \mathcal{B}} \mathbf{t} \cdot \mathbf{u} dA, \quad (2.2)$$

where  $\psi_0$  is the elastic energy density,  $G_c$  the Griffith's critical energy release rate — cf. [19],  $\boldsymbol{\varepsilon}$  the strain, and  $\mathbf{b}$  and  $\mathbf{t}$  are the body and surface forces, respectively.

## 2.1. Regularization of a sharp crack

Fig. 2 shows the crack phase field variable  $\phi(\mathbf{x}, t)$ , which is used to trace the crack propagation in the material such that the value  $\phi = 0$  represents the undamaged phase and the value  $\phi = 1$  represents the damaged phase (crack) and there is a smooth transition between the two phases in the interface. The regularization of the sharp crack  $\Gamma$  to diffused crack  $\Gamma_\ell$  is done as

$$\Gamma_\ell = \int_{\mathcal{B}} \gamma(\phi, \nabla\phi) dV, \quad \gamma(\phi, \nabla\phi) = \frac{1}{\ell} \left( \phi^2(1-\phi)^2 + \frac{\ell^2}{2} |\nabla\phi|^2 \right), \quad (2.3)$$

where  $\gamma(\phi, \nabla\phi)$  is the energy density function for the crack surface per unit volume of the body [16]. The length scale parameter  $\ell$  defines the width of the diffused crack Fig. 2.

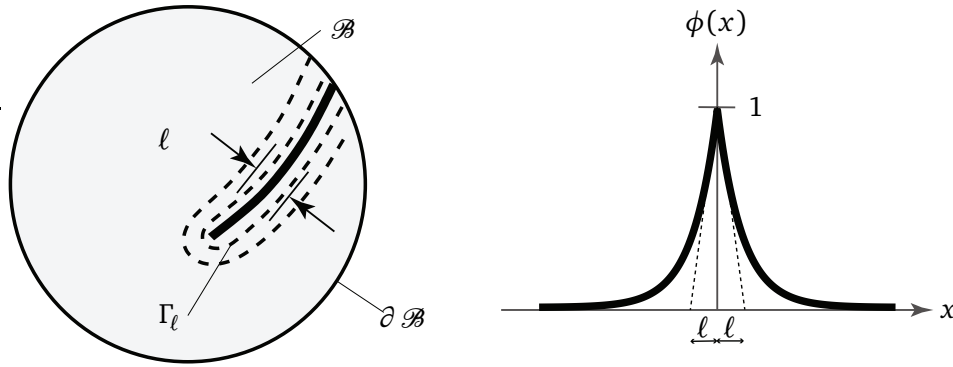


Figure 2: Crack phase field representation.

Considering the vanishing length scale  $\ell \rightarrow 0$ , the regularized crack  $\Gamma_\ell$  converges to a sharp crack  $\Gamma$ . For a sharp crack in the body, the crack phase field  $\phi(\mathbf{x})$  is derived by minimizing the diffused crack  $\Gamma_\ell$  with respect to the variable  $\phi$ . This leads to the Euler equation with Neumann boundary conditions — viz.

$$\begin{aligned} 2\phi + 4\phi^3 - 6\phi^2 - \ell^2 \Delta \phi &= 0, & \mathbf{x} \in \mathcal{B}, \\ \nabla\phi \cdot \mathbf{n} &= 0, & \mathbf{x} \in \partial\mathcal{B}. \end{aligned}$$

Substituting the energy density function for crack surface  $\gamma(\phi, \nabla\phi)$  of (2.3) in the fracture energy term  $\psi_f$  of (2.2) yields

$$\psi_f = \int_{\Gamma} G_c dA = \int_{\mathcal{B}} G_c \gamma(\phi, \nabla\phi) dV. \quad (2.4)$$

## 2.2. Governing differential equations

Since the phase field model uses a diffused crack smeared by the function  $\phi(\mathbf{x})$ , the elastic energy density function in the Eq. (2.2) degrades with the evolution of phase field

variable  $\phi$ . This process can be modelled by introducing an energy degradation function  $g(\phi)$  such that

$$\psi_s = \int_{\mathcal{B}} g(\phi) \psi_0(\boldsymbol{\varepsilon}) dV, \quad (2.5)$$

where

$$g(\phi) = (1 - 10\phi^3 + 15\phi^4 - 6\phi^5) + k, \quad \psi_0(\boldsymbol{\varepsilon}) = \frac{1}{2}\lambda \text{tr}^2(\boldsymbol{\varepsilon}) + \mu \text{tr}(\boldsymbol{\varepsilon}^2)$$

with the Lamé's constants  $\lambda$ ,  $\mu$  and a positive constant  $k$  that ensures a small stiffness value of  $k\psi_0$  when a fully damaged phase is reached for the phase field variable  $\phi = 1$ .

The strain energy density function  $\psi_0$  in the Eq. (2.5) propagates the crack even under compression. To facilitate the crack propagates under tension only, the elastic energy has to be decomposed into tensile and compressive parts. In addition, the degradation of the energy must be applied to tensile part of the elastic energy only — i.e.

$$\psi_s = \int_{\mathcal{B}} g(\phi) \psi_0^+(\boldsymbol{\varepsilon}) dV + \int_{\mathcal{B}} \psi_0^-(\boldsymbol{\varepsilon}) dV. \quad (2.6)$$

The terms  $\psi_0^+$  and  $\psi_0^-$  are defined by the spectral decomposition of the strain tensor  $\boldsymbol{\varepsilon}$ , viz.

$$\psi_0^\pm(\boldsymbol{\varepsilon}) = \frac{1}{2}\lambda(\text{tr}(\boldsymbol{\varepsilon}))_\pm^2 + \mu \text{tr}(\boldsymbol{\varepsilon}_\pm^2),$$

where

$$\boldsymbol{\varepsilon}_\pm := \sum_{i=1}^{\delta} \langle \varepsilon^i \rangle_\pm \mathbf{n}^i \otimes \mathbf{n}^i, \quad \langle \cdot \rangle_\pm := ((\cdot) \pm |\cdot|)/2,$$

and  $\delta \in \{1, 2, 3\}$  is the dimension of the problem,  $\text{tr}(\boldsymbol{\varepsilon}) = \sum_{i=1}^{\delta} \varepsilon_{ii}$  is the strain tensor trace or its first invariant, whereas  $\varepsilon^i$  and  $\mathbf{n}^i$  are the principal strains and the principal strain directions. We also note that  $\langle \cdot \rangle_\pm$  are the Macaulay brackets, so that  $\langle a \rangle_+$  is a filter for positive  $a$  and  $\langle a \rangle_-$  a filter for negative  $a$ .

Substituting the strain energy of (2.6), fracture energy of (2.4), and the energy related to external forces of (2.2) into the total energy functional (2.1) yields

$$\begin{aligned} E(\mathbf{u}, \phi) = & \int_{\mathcal{B}} g(\phi) \psi_0^+(\boldsymbol{\varepsilon}) dV + \int_{\mathcal{B}} \psi_0^-(\boldsymbol{\varepsilon}) dV \\ & + \int_{\mathcal{B}} G_c \gamma(\phi, \nabla \phi) dV - \int_{\mathcal{B}} \mathbf{b} \cdot \mathbf{u} dV - \int_{\partial \mathcal{B}} \mathbf{t} \cdot \mathbf{u} dA. \end{aligned} \quad (2.7)$$

Minimizing the total energy functional  $E(\mathbf{u}, \phi)$  from (2.7) with respect to the displacement field  $\mathbf{u}$  and the phase field  $\phi$  leads to the evolution equations

$$\nabla \cdot [g(\phi) \partial_{\boldsymbol{\varepsilon}} \psi_0^+ + \partial_{\boldsymbol{\varepsilon}} \psi_0^-] + \mathbf{b} = 0, \quad (2.8)$$

$$\Phi \phi - G_c \ell \nabla^2 \phi = 0, \quad (2.9)$$

where

$$\Phi(\phi, \psi_0^+) = \frac{2G_c}{\ell}(2\phi^2 - 3\phi + 1) + 30(2\phi^2 - \phi^3 - \phi)\psi_0^+,$$

and  $\partial_{\boldsymbol{\varepsilon}}$  is the partial derivative with respect to the strain  $\boldsymbol{\varepsilon}$ .

We observe that the tensile part of the elastic energy  $\psi_0^+$  drives the evolution of the phase field  $\phi$ . However, this form of the Eq. (2.9) does not ensure the increase of the phase field variable  $\phi$  along with the loading history. A history parameter  $H$  was introduced by Miehe *et al.* [16] to enforce the irreversibility of cracking. This parameter presents the maximum of the tensile part of the elastic energy in the loading history — i.e.

$$H(\mathbf{x}, t) = \max_{t \in [0, T]} \psi_0^+(\boldsymbol{\varepsilon}). \quad (2.10)$$

Replacing  $\psi_0^+$  in the Eq. (2.9) by the history parameter  $H$ , we write the phase field evolution equation as

$$\Phi(\phi, H)\phi - G_c \ell \nabla^2 \phi = 0. \quad (2.11)$$

### 3. Numerical Implementation

The introduction of the history parameter  $H$  allows to decouple the evolution equations and use a staggered approach in approximation methods. However, the splitting of the elastic energy density brings a non-linearity to the Eq. (2.8) and leads to a higher computational time. In order to overcome this problem, a hybrid formulation is used, so that the linear balance of momentum equation is retained for the evolution of displacement and the evolution of the phase field  $\phi$  is still driven by the tensile part of the elastic energy density  $\psi_0^+$ . As the result, the final strong form of the governing equation for displacements can be written as

$$\nabla \cdot [g(\phi)\partial_{\boldsymbol{\varepsilon}}\psi_0] + \mathbf{b} = 0. \quad (3.1)$$

We also note that in order to prevent the crack surface interpenetration, at any point  $\mathbf{x}$  the phase field  $\phi$  should be set as zero if  $\psi_0^+ < \psi_0^-$ .

#### 3.1. Weak form of governing equations

The weak form of the governing equations (3.1) and (2.11) is obtained by multiplying them with weight functions ( $w_u$  and  $w_\phi$ ) and integrating over the body  $\mathcal{B}$ , i.e.

$$\begin{aligned} \int_{\mathcal{B}} w_u \{ \nabla \cdot [g(\phi)\partial_{\boldsymbol{\varepsilon}}\psi_0] + \mathbf{b} \} dV &= 0, \\ \int_{\mathcal{B}} w_\phi [ \Phi(\phi, H)\phi - G_c \ell \nabla^2 \phi ] dV &= 0. \end{aligned}$$

Note that since  $\psi_0 = (1/2)\boldsymbol{\varepsilon} : \mathcal{C} : \boldsymbol{\varepsilon}$ , we have  $\partial_{\boldsymbol{\varepsilon}}\psi_0 = \mathcal{C} : \boldsymbol{\varepsilon}$ , where  $\mathcal{C}$  is a constitutive matrix. Thus the final weak form is

$$\int_{\mathcal{B}} [g(\phi)\nabla w_u \mathcal{C} : \boldsymbol{\varepsilon} + w_u \mathbf{b}] dV = 0, \quad (3.2)$$

$$\int_{\mathcal{B}} [\Phi(\phi, H)w_\phi \phi + G_c \ell \nabla w_\phi \nabla \phi] dV = 0. \quad (3.3)$$

### 3.2. Finite element approximations

The unknown displacement field and the phase field are approximated by the standard Bubnov-Galerkin method with the same shape function for both variables. The domain  $\mathcal{B}$  is discretized into  $n_{el}$  finite elements  $\mathcal{B}_0^e$  and each element has  $n$  number of nodes. Note that for each finite element  $\mathcal{B}_0^e$  we use the following approximations:

$$\begin{aligned} \mathbf{u} &= \sum_{I=1}^n \mathbf{N}_I \cdot \mathbf{u}_I, & \phi &= \sum_{I=1}^n N_I \phi_I, \\ \boldsymbol{\varepsilon} &= \sum_{I=1}^n \mathbf{B}_I^u \cdot \mathbf{u}_I, & \nabla \phi &= \sum_{I=1}^n \mathbf{B}_I \phi_I, \end{aligned}$$

where  $\mathbf{N}_I$  is the shape function diagonal matrix having nodal shape functions  $N_I$  as components,  $\mathbf{B}_I^u$  the standard strain-displacement matrix,  $\mathbf{B}_I$  the derivative of the shape function, and  $\mathbf{u}_I$  and  $\phi_I$  are the displacement and phase field values at the nodes. Similar approximations are used for the weights  $w_u$  and  $w_\phi$  and their gradients  $\nabla w_u$  and  $\nabla w_\phi$ .

Substituting the above approximations in the Eqs. (3.2) and (3.3) leads to the residual vectors

$$\begin{aligned} \mathbf{R}_I^u &= \mathbf{A} \int_{\mathcal{B}_0^e} [g(\phi)(\mathbf{B}_I^u)^T : \mathcal{C} : \boldsymbol{\varepsilon} + \mathbf{N}_I^T \cdot \mathbf{b}] dV, \\ \mathbf{R}_I^\phi &= \mathbf{A} \int_{\mathcal{B}_0^e} [\Phi(\phi, H)N_I^T \phi + G_c \ell \mathbf{B}_I^T \phi] dV, \end{aligned}$$

with the symbol  $\mathbf{A}$  representing the assembling operator such that all local element data are assembled from 1 to  $n_{el}$ .

The stiffness matrices corresponding to  $\mathbf{u}$  and  $\phi$  are obtained by the linearization of the residual vectors and have the form

$$\begin{aligned} \mathbf{K}_{IJ}^{uu} &= \frac{\partial \mathbf{R}_I^u}{\partial \mathbf{u}_J} = \mathbf{A} \int_{\mathcal{B}_0^e} [g(\phi)(\mathbf{B}_I^u)^T : \mathcal{C} : \mathbf{B}_J^u] dV, \\ \mathbf{K}_{IJ}^{\phi\phi} &= \frac{\partial \mathbf{R}_I^\phi}{\partial \phi_J} = \mathbf{A} \int_{\mathcal{B}_0^e} [\Phi(\phi, H)N_I^T N_J + G_c \ell \mathbf{B}_I^T : \mathbf{B}_J] dV. \end{aligned}$$

These stiffness matrices are symmetric and positive-definite, so that all eigenvalues are positive [4]. The order of these matrices corresponds to the total unknowns in the complete solution. The stiffness matrix should not be singular because in this case it is not possible to construct the inverse matrix and obtain the solution.

The linearized finite element system below, have to be solved by the Newton-Raphson method

$$\begin{bmatrix} \mathbf{K}^{uu} & 0 \\ 0 & \mathbf{K}^{\phi\phi} \end{bmatrix} \begin{bmatrix} \Delta \mathbf{u} \\ \Delta \phi \end{bmatrix} = - \begin{bmatrix} \mathbf{R}^u \\ \mathbf{R}^\phi \end{bmatrix}.$$

Although this method has been already applied to the above nonlinear system, the presence of the gradient term requires the use of a fine mesh in the path of crack propagation and increases the computational time. To speed up the convergence, one can exploit the Jacobi-free Newton-GMRES method [2] or the Newton-HSS iteration method [3,5]. It has not been done here but will be considered elsewhere.

### 3.3. Staggered algorithm

A robust staggered algorithm is used to solve the coupled equilibrium equations (3.1) and the phase field evolution equation (2.11). We use the displacement, history parameter and the crack phase field variable from the previous step  $n$  as the input, whereas at the first step the initial values are employed. At the next step, we use the history parameter  $H^{n+1}$  obtained from the Eq. (2.10). As soon as the history parameter is updated, algebraic equations

$$[\mathbf{K}^{\phi\phi}]\{\Delta\phi\} = -\{\mathbf{R}^\phi\}$$

are solved by the iterative Newton-Raphson method until the phase field variable

$$\phi^{n+1} = \phi^n + \Delta\phi$$

converges. Establishing this phase field variable, we solve the algebraic equations

$$[\mathbf{K}^{uu}]\{\Delta\mathbf{u}\} = -\{\mathbf{R}^u\}$$

by the Newton-Raphson iteration scheme and determine the displacement

$$\mathbf{u}^{n+1} = \mathbf{u}^n + \Delta\mathbf{u}.$$

Thus, the converged values of displacement and phase field variable are obtained for the  $(n + 1)$  step. The procedure is repeated until convergence. The final reaction force versus displacement curve and fracture pattern based on crack phase field is plotted.

---

#### Algorithm 3.1 Staggered Approach.

---

**Result:** Compute  $\mathbf{u}^{n+1}$ ,  $H^{n+1}$  and  $\phi^{n+1}$ .

Initialize displacement  $\mathbf{u}^n$ , history parameter  $H^n$  and phase field fracture  $\phi^n$ .

**while**  $STEP \leq NSTEP$  **do**

    Update history field  $H^{n+1}$ .

    Compute  $\mathbf{K}^{\phi\phi}$  and  $\mathbf{R}^\phi$ .

```

if  $|\mathbf{R}^\phi| > \textit{tolerance}$  then
  Solve for  $\phi$  using  $[\mathbf{K}^{\phi\phi}]\{\Delta\phi\} = -\{\mathbf{R}^\phi\}$ ;
   $\phi^{n+1} = \phi^n + \Delta\phi$ ;
else
   $\phi^{n+1} = \phi^n$ .
end if
Compute  $\mathbf{K}^{uu}$  and  $\mathbf{R}^u$ .
if  $|\mathbf{R}^u| > \textit{tolerance}$  then
  Solve for  $\mathbf{u}$  using  $[\mathbf{K}^{uu}]\{\Delta\mathbf{u}\} = -\{\mathbf{R}^u\}$ ;
   $\mathbf{u}^{n+1} = \mathbf{u}^n + \Delta\mathbf{u}$ ;
else
   $\mathbf{u}^{n+1} = \mathbf{u}^n$ .
end if
end while

```

---

#### 4. Phase Field Fracture Model

To demonstrate the work of the proposed phase field model, a standard benchmark problem has been considered. We consider a plane strain plate specimen having a single edge crack at one side in the first example and a plate with an asymmetric double edge crack on both sides in the second example to show the different types of failure encountered.

##### 4.1. Plate with single edge crack

A plate specimen with dimensions of  $1 \times 1$  mm is considered having a single edge crack at the center of length 0.5 mm is subjected to tensile loading as shown in Fig. 3.

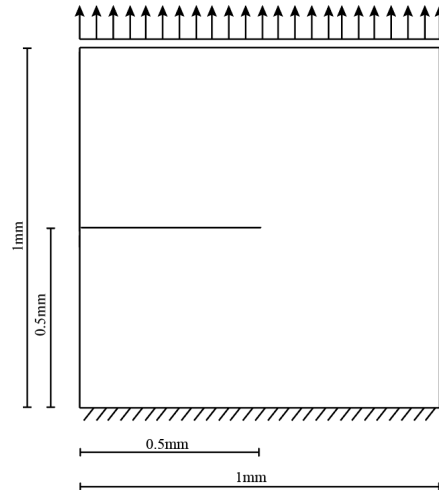


Figure 3: Geometry of the plate with single edge crack.

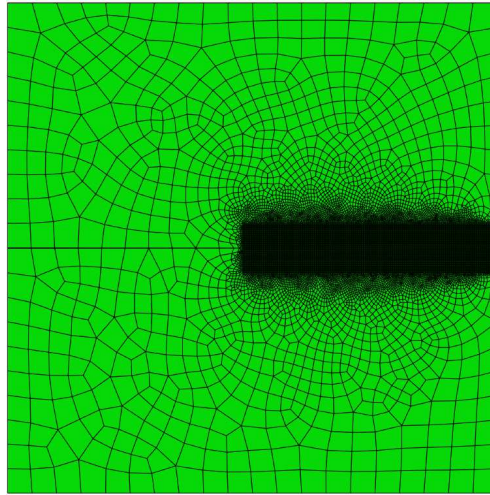


Figure 4: Mesh pattern of the plate with single edge crack.

The material properties taken are Young’s modulus  $E = 210 \text{ kN/mm}^2$ , Poisson’s ratio  $\mu = 0.3$  and  $G_c = 0.0027 \text{ kN/mm}$ . A sufficiently refined unstructured mesh of 18,868 elements is considered for the analysis as shown in Fig. 4. The reaction force versus the displacement graph is plotted for various length scales with the displacement and time steps constant as shown in Fig. 5. Two different length scales  $l = 0.0025\text{mm}$  and  $l = 0.015\text{mm}$  were considered for the analysis. It is observed that in the reaction force versus displacement plot the peak reaction force values are decreasing with increasing length scale and also the displacement at failure is decreasing. The crack paths are as shown in Figs. 6 and 7 for the various length scales considered. The contour index for the damage variable  $\phi$  is provided

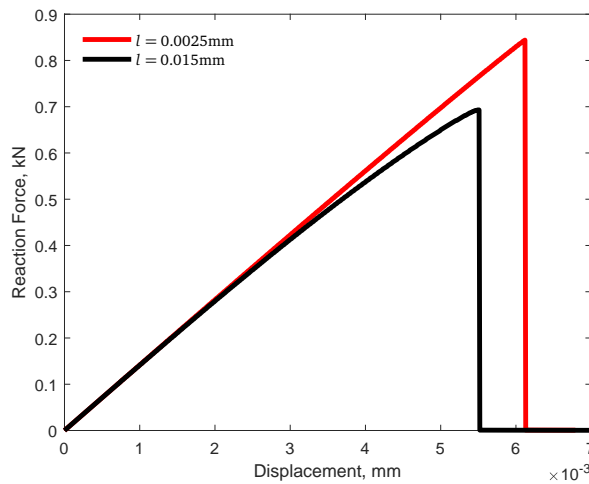


Figure 5: Reaction force-Displacement plot for the plate with single edge crack.

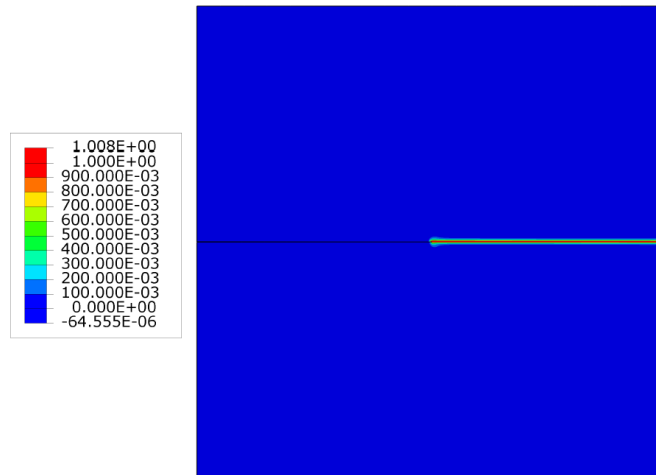


Figure 6: Crack propagation in plate with single edge crack for  $l = 0.0025\text{mm}$ .

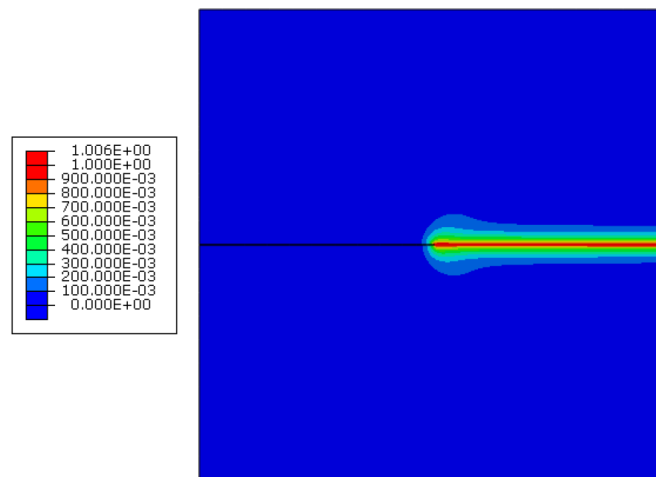


Figure 7: Crack propagation in plate with single edge crack for  $l = 0.015\text{mm}$ .

next to the figures. The contour value of 1 indicates the crack. It can be observed that the width of the crack increases with increasing length scale in conjunction with the crack phase field regularization as described in Section 2.

#### 4.2. Plate with asymmetric double edge crack

Consider the  $40 \times 40\text{mm}$  plate with the edge cracks of length  $8\text{mm}$  on both sides having an eccentricity of  $2\text{mm}$  between them at the center and subjected to the tensile loading as in Fig. 8. As far as the material characteristics are concerned, we use the Young's modulus  $E = 210 \text{ kN/mm}^2$ , the Poisson's ratio  $\mu = 0.3$ , and  $G_c = 0.0027 \text{ kN/mm}$ . The refined

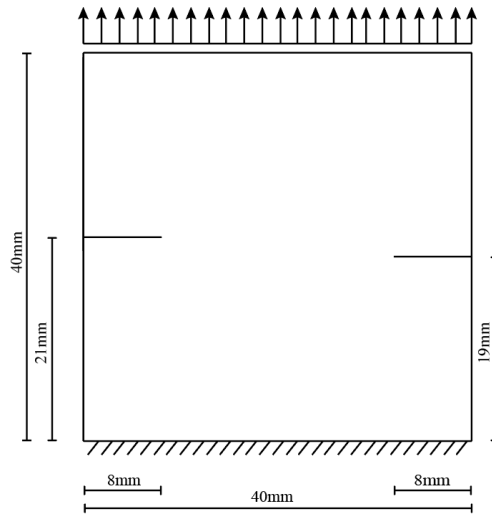


Figure 8: Geometry of the plate with asymmetric double edge crack.

unstructured mesh of 27,720 elements shown in Fig. 9, and the graphs of reaction force versus displacement for various length scales with constant displacements and time steps are presented in Fig. 10. We note that this trend is similar to the one in the previous example. However, at higher length scales the peak force and the displacement at failure are almost the same. The crack paths for various length scales are shown in Figs. 11-13, with the contour index for the damage variable  $\phi$  attached to the corresponding figures. Similar effects concerning the crack width are also visible. In addition, example demonstrates the crack merging simulation.

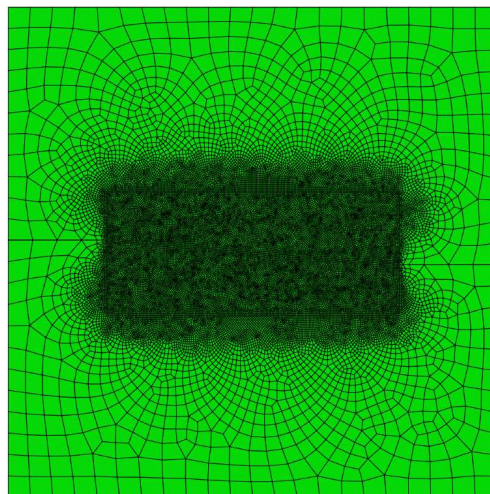


Figure 9: Mesh pattern of the plate with asymmetric double edge crack.

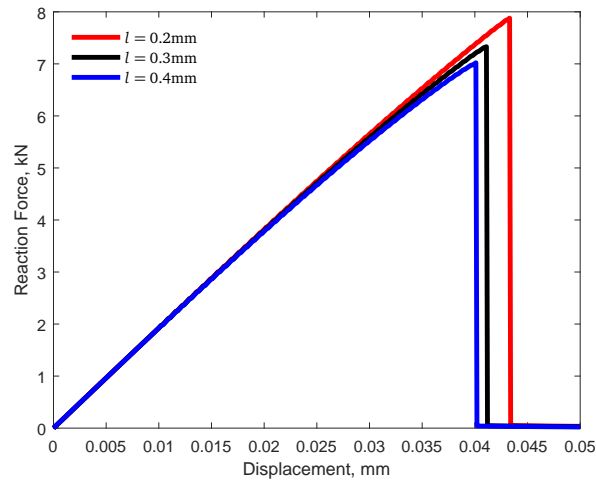


Figure 10: Reaction force-Displacement plot for plate with asymmetric double edge crack.

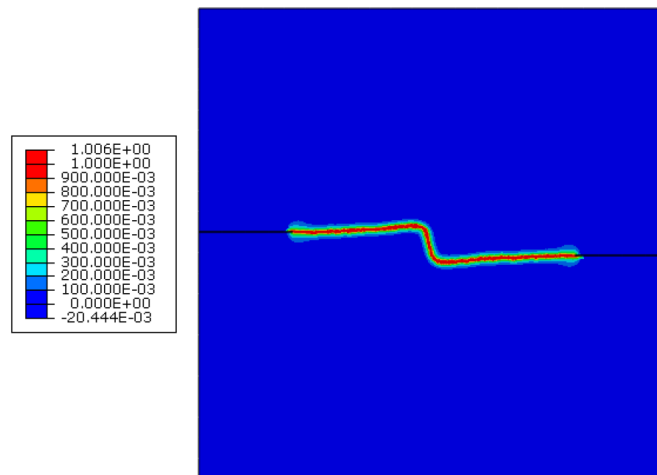


Figure 11: Crack propagation in plate with asymmetric double edge crack for  $l = 0.2\text{mm}$ .

## 5. Conclusion

A thermodynamically consistent nonlocal phase field model for fracture has been presented. The solution of phase field models requires mathematical and numerical techniques. We use variational calculus to minimize the total energy functional and obtain the governing differential equations. The equations are solved by a finite element scheme. The fracture energy term consists of a gradient term which has a length scale parameter as a coefficient. This makes it a nonlocal model and leads to a better regularization of the fracture problem. The minimization of the total energy functional with respect to displacements produces an equilibrium equation. Besides, the minimization of the total energy

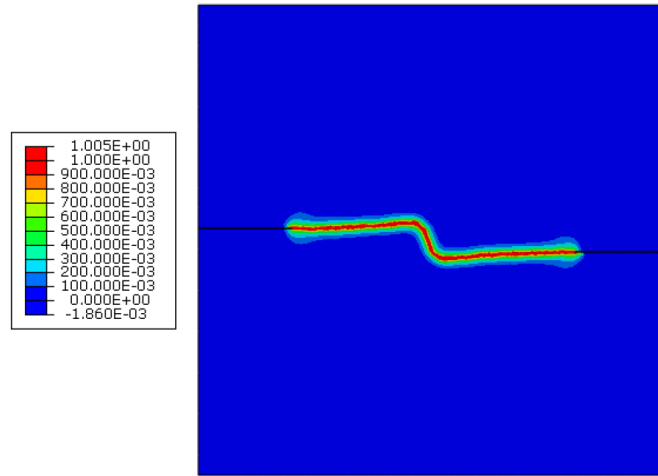


Figure 12: Crack propagation in plate with asymmetric double edge crack for  $l = 0.3\text{mm}$ .

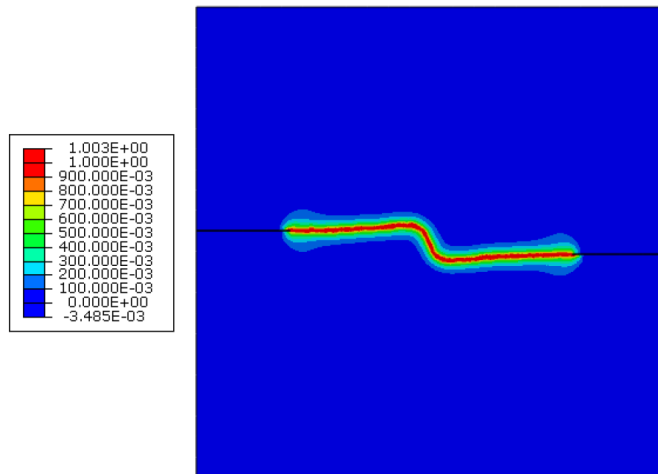


Figure 13: Crack propagation in plate with asymmetric double edge crack for  $l = 0.4\text{mm}$ .

functional with respect to phase field variable yields the Allen-Cahn evolution equation for crack propagation.

The performance of the phase field fracture model is illustrated by numerical examples. We note that this model is able to predict crack deviations. Merging up of two cracks into one is also been demonstrated.

### Acknowledgments

The authors would like to thank the Department of Science and Technology (DST)-Russian Foundation for Basic Research (RFBR) International Cooperation Divisions for fund-

ing this project at the initial stage. The second and third authors also thank the Government of the Russian Federation (Contract No. 075-15-2019-1928).

## References

- [1] M. Ambati, T. Gerasimov and L. De Lorenzis, *A review on phase-field models of brittle fracture and a new fast hybrid formulation*, *Comput. Mech.* **55**, 383–405 (2015).
- [2] H.-B. An and Z.-Z. Bai, *A globally convergent Newton-GMRES method for large sparse systems of nonlinear equations*, *Appl. Numer. Math.* **57**(3), 235–252 (2007).
- [3] Z.-Z. Bai and X.-P. Guo, *On Newton-HSS methods for systems of nonlinear equations with positive-definite Jacobian matrices*, *J. Comput. Math.* **28**(2), 235–260 (2010).
- [4] Z.-Z. Bai and J.-Y. Pan, *Matrix Analysis and Computations*, SIAM (2021).
- [5] Z.-Z. Bai and X. Yang, *On HSS-based iteration methods for weakly nonlinear systems*, *Appl. Numer. Math.* **59**(12), 2923–2936 (2009).
- [6] Z.-P. Bažant and J. Planas, *Fracture and Size Effect in Concrete and Other Quasibrittle Materials*, CRC Press (1997).
- [7] T. Belytschko, H. Chen, J. Xu and G. Zi, *Dynamic crack propagation based on loss of hyperbolicity and a new discontinuous enrichment*, *Int. J. Numer. Methods Eng.* **58**(12), 1873–1905 (2003).
- [8] M.J. Borden, T.J.R. Hughes, C.M. Landis and C.V. Verhoosel, *A higher-order phase-field model for brittle fracture: Formulation and analysis within the isogeometric analysis framework*, *Comput. Methods Appl. Mech. Eng.* **273**, 100–118 (2014).
- [9] B. Bourdin, G.A. Francfort and J.-J. Marigo, *Numerical experiments in revisited brittle fracture*, *J. Mech. Phys. Solids.* **48**(4), 797–826 (2000).
- [10] R. de Borst, *Numerical aspects of cohesive-zone models*, *Eng. Fract. Mech.* **70**(14), 1743–1757 (2003).
- [11] G.A. Francfort and J.-J. Marigo, *Revisiting brittle fracture as an energy minimization problem*, *J. Mech. Phys. Solids* **46**(8), 1319–1342 (1998).
- [12] A.-A. Griffith, *VI. The phenomena of rupture and flow in solids*, *Philosophical Transactions of the Royal Society of London, Series A, Containing Papers of a Mathematical or Physical Character* **221**, 163–198 (1921).
- [13] C.-S. Han, *Influence of the molecular structure on indentation size effect in polymers*, *Mater. Sci. Eng. A* **527**(3), 619–624 (2010).
- [14] S. Karthik, A. Rajagopal and J.N. Reddy, *Nonlocal phase field approach for modeling damage in brittle materials*, *Mech. Mater.* **157**, 103797 (2021).
- [15] P. Kasirajan, S. Bhattacharya, A. Rajagopal, and J.N. Reddy, *Phase field modeling of fracture in quasi-brittle materials using natural neighbor Galerkin method*, *Comput. Methods Appl. Mech. Engrg.* **366**, 113019 (2020).
- [16] C. Miehe, M. Hofacker and F. Welschinger, *A phase field model for rate-independent crack propagation: Robust algorithmic implementation based on operator splits*, *Comput. Methods Appl. Mech. Eng.* **199**(45-48), 2765–2778 (2010).
- [17] P. Raghu, A. Rajagopal and J.N. Reddy, *Thermodynamically consistent variational approach for modeling brittle fracture in thick plates by a hybrid phase field model*, *J. Appl. Mech.* **87**(2), 021002 (2020).
- [18] J.-Y. Wu, V.-P. Nguyen, C.-T. Nguyen, D. Sutula, S. Sinaie and S. Bordas, *Phase-field modeling of fracture*, *Adv. Appl. Mech.* **53**, 1–183 (2020).
- [19] A.-T. Zehnder, *Fracture Mechanics*, Springer (2012).